Comput Mech
DOI 10.1007/s00466-017-1414-3

ORIGINAL PAPER

Modeling and rapid simulation of the propagation and multiple branching of electrical discharges in gaseous atmospheres

T. I. Zohdi[1]

Received: 12 February 2017 / Accepted: 18 April 2017

Abstract The trajectories and branching of electrical discharges through gaseous atmospheres, such as lightning and coronal emissions from high-voltage electromachinery, are of interest in a variety of applications. Multiple branches can evolve in an initially poor atmospheric conductor when a strong electrical discharge builds up, then propagates through the atmosphere by *dielectric breakdown*. Multiple branches can be generated in gases because of the disordered character of the media at the microscale, with an overall influence occurring from the ambient electric fields. In this paper, we develop a sufficiently flexible computational model to describe discharge trajectory and branching. The framework allows analysts to rapidly simulate thousands of electrical discharge scenarios, in order to statistically explore the dependency of the overall system behavior on the relevant physical parameters.

Keywords Electrical discharge · Atmospheres · Propagation · Branching

1 Electrical discharges in gaseous atmospheres

The trajectory and branching of an electrical discharge in a gaseous atmosphere is of interest to industry and the natural sciences (Figs. 1, 2). Relevant, wide ranging, applications are (1) lightning, (2) end-coronal insulation protection in high-voltage electromachinery, such as industrial-scale generators and (3) controlled electrical ignition in internal combustion engines. The most common naturally occurring electrical discharge in a gas is lightning. It is believed that ice formation within a cloud causes positive and negative charge separation, producing a potential difference between the Earth and the lower cloud portion, leading to a possible electrical discharge. One school of thought proposes that a discharge will occur due to electrostatic induction, under the assumption that charge separation occurs in conjunction with strong updrafts that carry supercooled water droplets upwards, which then collide with ice crystals to form "graupel", which is a soft ice-water mixture. This results in negative charged graupel and positive charged ice crystals. Updrafts drive the less heavy ice crystals upwards, causing the upper portion of the cloud to attain a positive charge, while gravity causes the heavier negatively charged graupel to fall to lower portions of the cloud, building up a negative charge. The process of charge separation and accumulation continues until the electrical potential becomes strong enough to initiate a lightning discharge.[1] Another school of thought asserts that droplets of ice and rain become electrically polarized as they fall through the Earth's natural electric field and the colliding ice particles become charged by electrostatic induction. There are many other influencing factors cited in the literature, such as humidity, pressure, solar induced activity, gamma ray bursts (leading to ionization of air molecules), volcanic dust, intense forest fires, etc. Detailed discussions can be found in Rakov and Uman [1], Demirkol et al. [2], Uman [3], Fishman et al. [4], Inan et al. [5] and Inan and Inan [6]. The physics of lightning is virtually identical to

✉ T. I. Zohdi
zohdi@me.berkeley.edu

[1] Department of Mechanical Engineering, 6195 Etcheverry Hall, University of California, Berkeley, CA 94720-1740, USA

[1] Lightning travels between 2×10^5–10^6 m/s with an average current between 100 and 200 amperes and a peak of 1000–2000 amperes. For comparison purposes, a light bulb operates at one ampere, while a typical electrical socket operates at 15 amperes.

Published online: 03 May 2017

Fig. 1 Pictures of various discharge scenarios from natural causes (lightning). Photos available courtesy of the public domain site https://pixabay.com/en/lightning-storm-weather-sky-399853/ and https://pixabay.com/en/flashes-thunderstorm-electricity-500447/

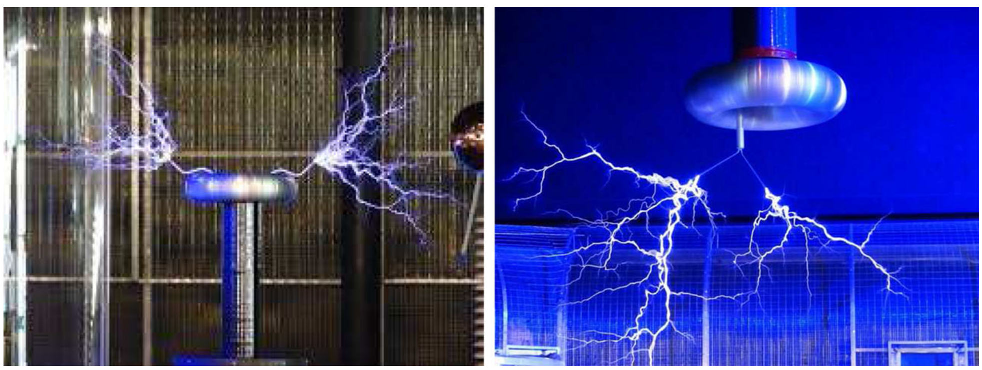

Fig. 2 Pictures of various discharge scenarios from Tesla coils. Photo available courtesy of the public domain site https://pixabay.com/en/flash-tesla-coil-experiment-113310/ and https://pixabay.com/en/flash-tesla-coil-experiment-113302/

electrical discharges in high-voltage electromachinery. The understanding of discharge trajectories is critical to end-corona insulation (protection) systems, in order to mitigate harmful electrical discharges. See for example, Staubach et al. [7–10], Mcdermid [11], Merouchi et al. [12,13], Schmerling et al. [14], Weida et al. [15], Day et al. [16], Kogan et al. [17], Liu and Xu [18], Taylor [19], Krpal and Kuerov [20], Sumereder et al. [21], Hudon and Rehder [22], Abdel-Salam and Shamloul [23], Litinsky et al. [24], Guastavino et al. [25], Ou and Techaumnat [26], Bouhaouche et al. [27], Nazir and Phung [28], Zohdi [29–33]. Another related application is the development of precisely-controlled electrical ignition systems for ultra lean fuels such as ethanol (see Azevedo et al. [34] and Schwartz [35]). Recent advancements in the real time adjustment controls for in-situ ignition systems is becoming viable. Such approaches are important for further development of next-generation Compression Ignition Direct Injection (CIDI) and Homogeneous Charge Compression Ignition (HCCI) engines. Such systems can lead to improved efficiency by igniting ultra lean fuels at low temperatures, where standard compression engines are limited and misfiring can occur. We refer the interested reader to Ikeda et al. [36,37], Leipold et al. [38], Phelps [39], Aleiferis et al. [40], Johansson [41], Kogoma [42], Phuoc [43,44], Morsy et al. [45,46], Ma et al. [47,48], Mohamed et al. [49], Weinberg and Wilson [50], Dale et al. [51], Ronney [52], Beduneau et al. [53], Chen and Lewis [54], Kim et al. [55], Ombrello and Ju [56], Mintoussov et al. [57], Korolev and Matveev [58], Esakov et al. [59], Linkenheil et al. [60,61], Kawahara et al. [62], Mehresh et al. [63], Bogin et al. [64] and Prager et al. [65]. A further understanding of what influences the propagation of electrical discharges in all of the mentioned applications is important.

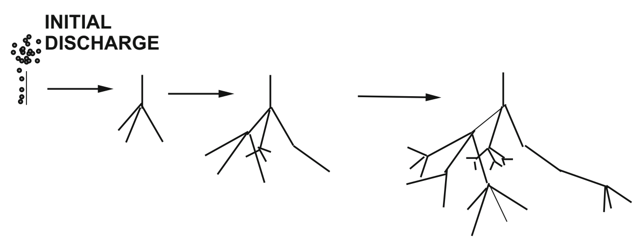

Fig. 3 Growth of branches from an initial discharge branch

To a large degree, the discharge trajectory propagation is influenced by microscale events that transpire at the discharge front, where a charge buildup occurs and then "plows' through the gas, producing many branches, due to the disordered random nature of such media. The branching pathways

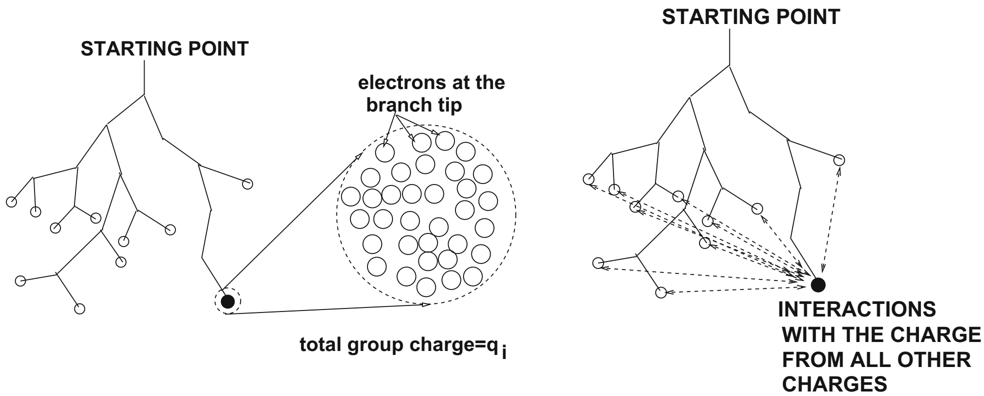

Fig. 4 Interaction of a branch endpoint with all others at an instant in time. All other charges also experience interactions with all other endpoints in a similar manner, as well as with external sources

that the discharge may take are in part determined by *dielectric breakdown* whereby, for sufficiently strong electrical fields, an initially poorly conducting gaseous medium can become an extremely good conductor. The process initiates from a sufficiently strong charge build-up which can accelerate free electrons that are present in a gas until they attain high enough energies to dislodge other electrons in initially neutral gas molecules. The process then repeats itself in a chain-reaction-like manner that results in the evolution of multiple pathways (branches). The investigation of dielectric breakdown dates back at least to Townsend [66], with detailed discussions found in, for example, Inan and Inan [6]. *In this work we do not focus on the discharge origin, but concentrate on developing a sufficiently flexible computational model to describe discharge trajectory and branching* (Fig. 3).

2 Governing equations

We consider an instant in time t when $i = 1, 2, 3, \ldots, N$ branch endpoints exist, each containing a charge q_i with a mass m_i. The dynamics of the endpoint of each branch, where each charge has built up, is governed by the basic equation of electrodynamics (Fig. 4)[2]

$$m_i \dot{\boldsymbol{v}}_i = q_i \left(\boldsymbol{E}^{ext}(\boldsymbol{r}_i) + \sum_{j=1, j \neq i}^{N} \boldsymbol{E}_j(\boldsymbol{r}_i) \right), \tag{2.1}$$

where $\boldsymbol{r}_i$ is the location of the branch endpoint, $\boldsymbol{v}_i$ is the velocity of the discharge and $\boldsymbol{E}^{ext}(\boldsymbol{r}_i)$ is the external ambient electric field of the environment acting at the point $\boldsymbol{r}_i$ and $\boldsymbol{E}_j(\boldsymbol{r}_i)$ is the electric field induced by branch tip j on branch tip i. We assume that the mass and charge of each branch is concentrated at the endpoint where the build up occurs via dielectric breakdown, and that any other induced electric fields are due to the charges in the other branches and external sources (power sources, Earth, etc), all of which will be superposed to produce the righthand side of Eq. 2.1.

3 Electric fields due to surrounding branches

Consider an electric field generated by the jth branch (Fig. 4), where the entire charge of that branch is aggregated as a point source at the end of the branch (during dielectric breakdown buildup phase), governed by Gauss' law (A and V being the surface area and volume encompassing the charge):

$$\underbrace{\int_A \boldsymbol{D} \cdot \boldsymbol{n}\, dA}_{=\epsilon E 4\pi ||\boldsymbol{r}-\boldsymbol{r}_j||^2} = \int_V Q\, dV = q_j, \tag{3.1}$$

where $\boldsymbol{D}$ is the electric field flux, ϵ is the atmospheric electric permittivity, $\boldsymbol{E}$ is the electric field ($||\boldsymbol{E}|| = E$), Q is the charge per unit volume, q_j is the total charge in the jth branch, leading to

$$\boldsymbol{E} = \frac{q_j}{4\pi\epsilon ||\boldsymbol{r} - \boldsymbol{r}_j||^2} \boldsymbol{n}_j, \tag{3.2}$$

where $\boldsymbol{n}_j$ is the normal-outward unit vector and $||\boldsymbol{r} - \boldsymbol{r}_j||$ is the distance from the jth branch point source to any point in the system ($\boldsymbol{r}$). Branch-to-branch interaction has a tendency, because of the like charges in branches, to spread out the branches.

4 Trajectory cone

We refer to the branches that will grow from the tip of a branch as "subbranches". The forward momentum of the

[2] We ignore magnetic fields.

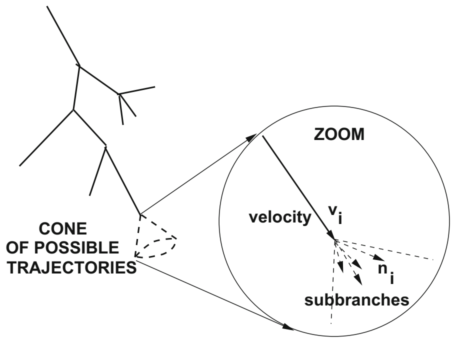

Fig. 5 Cone of feasible subbranch trajectories

charge (Eq. 2.1) in a branch biases the directions of the subbranches that are feasible at a tip. In order to take this into account, we adopt the following cone-like constraint (Fig. 5):

$$\frac{\boldsymbol{v}_i}{||\boldsymbol{v}_i||} \cdot \boldsymbol{n}_i \geq tol, \tag{4.1}$$

where $\frac{\boldsymbol{v}_i}{||\boldsymbol{v}_i||}$ is the previous direction of the branch, $\boldsymbol{n}_i$ is a possible direction of a subbranch, and $-1 \leq tol \leq 1$. A high positive value of "tol" indicates that the new branch direction is highly aligned with the previous main branch direction, while negative values indicate the branch could move backwards.

Remark Algorithmically, the number of subbranches that arise at a tip is determined by multiplying the charge by a random number between 0 and 1. A random path is also generated, within the feasible cone of trajectories, and the charge is assigned to that random path. This produces one subbranch. The process is then repeated for the remainder of that charge charge in that tip (producing more subbranches) until the charge remaining is depleted. This is done at each tip.

5 Algorithm

The algorithm is as follows (after setting the initial total discharge):

1. For each branch, the compute electric field from external sources and other surrounding branches.
2. For each branch, compute discharge "subbranches" by creating a random set of subbranches at the branch tip and distributing the branch charge among them, within the feasible trajectory cone.
3. For each branch, compute the trajectory of each new subbranch (velocity and position) by numerically solving Equation 2.1:

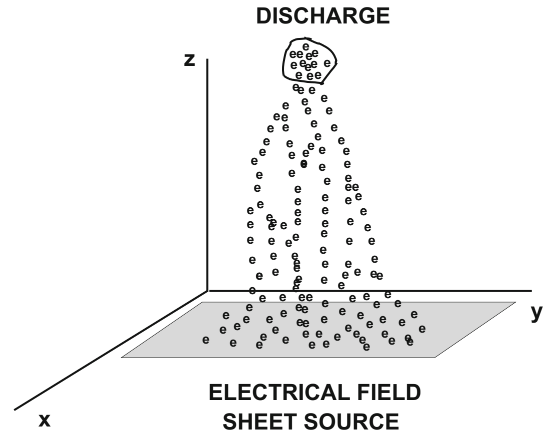

Fig. 6 Example of a sheet-source term

$$\dot{\boldsymbol{v}}_k \approx \frac{\boldsymbol{v}_k(t+\Delta t) - \boldsymbol{v}_k(t)}{\Delta t} = \frac{q_k}{m_k}\left(\boldsymbol{E}^{ext}(t) + \sum_{j=1, j\neq k}^{N} \boldsymbol{E}_j(\boldsymbol{r}_k(t))\right), \tag{5.1}$$

yielding the following update formula

$$\boldsymbol{v}_k(t+\Delta t) = \boldsymbol{v}_k(t) + \frac{q_k \Delta t}{m_k} \times\left(\boldsymbol{E}^{ext}(t) + \sum_{j=1, j\neq i}^{N} \boldsymbol{E}_j(\boldsymbol{r}_k(t))\right), \tag{5.2}$$

and for the position, $\dot{\boldsymbol{r}}_k = \boldsymbol{v}_k$, we have

$$\boldsymbol{r}_k(t+\Delta t) = \boldsymbol{r}_k(t) + \Delta t \boldsymbol{v}_k(t). \tag{5.3}$$

4. Increment time forward and repeat the procedure.

Remark 1 To the knowledge of the author, there are no such models of this phenomena in the literature, which has extensively been studied in the preparation of this publication.

Remark 2 It the upcoming simulations, the simulations were run with extremely time-steps, then repeatedly re-run with even finer time steps until there were negligible changes between refinements. The time-step size threshold that met this criteria, for all of the simulations, was adopted. Therefore, the simulations can be essentially free of numerical error. Because of the relatively simple structure of the equations, the simulations were all run of a Mac Powerbook Laptop in a matter of seconds, thus making the model ideal for parameter studies.

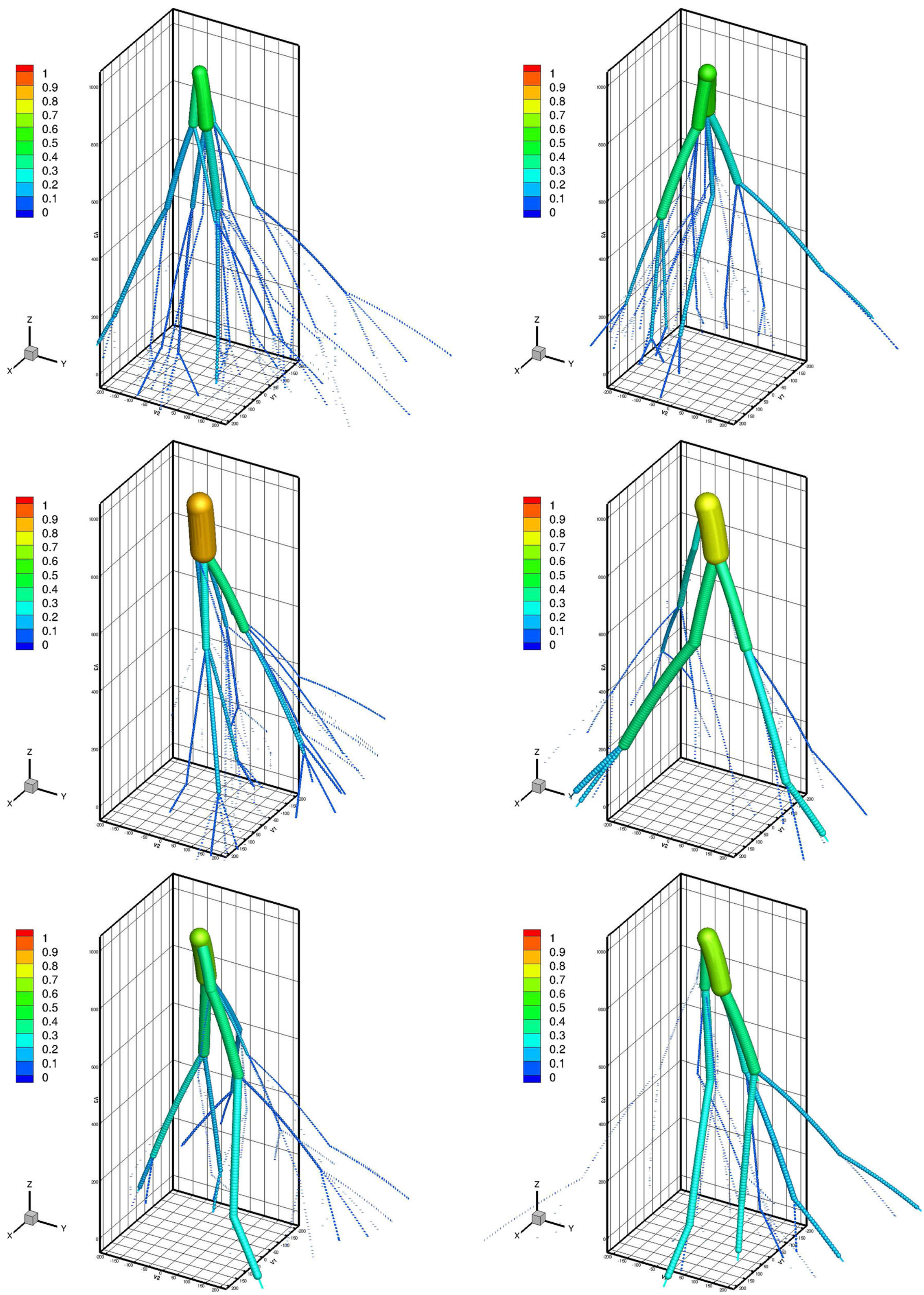

Fig. 7 Six different realizations of branches for a discharge of $q_D = -10^{-3}$ C and flat surface charge of $q_A = 10^{-1}$ C. The *color scale* indicates the magnitude of the charge relative to the original total discharge magnitude, as well as the charge-size-dependent spherical markers. (Color figure online)

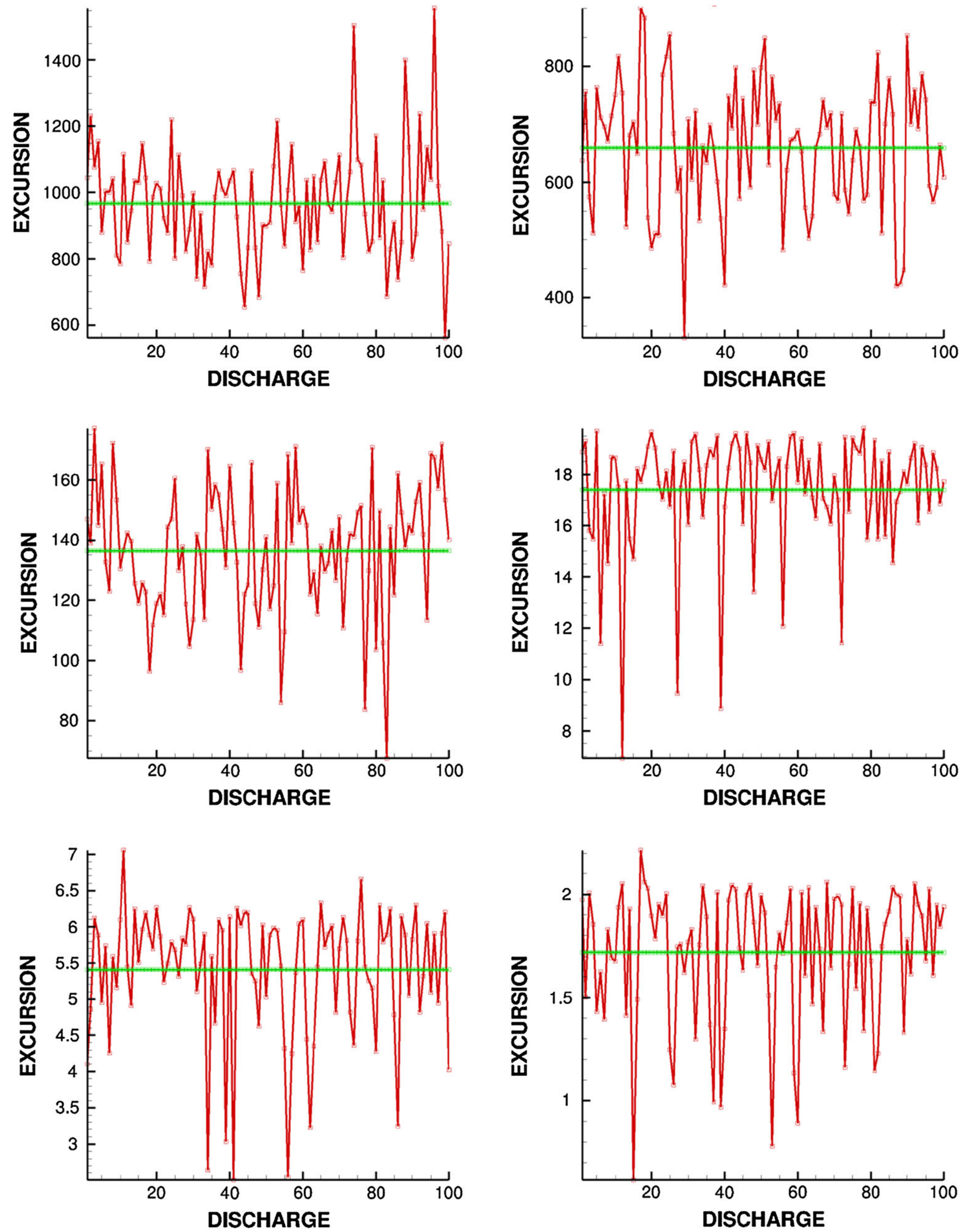

Fig. 8 Maximum excursion from z-axis ($\mathcal{R}$) for 100 discharges (random pathway realizations) with the sheet charge varied: $q_A = 10^{-2}, 10^{-1}, 1, 10, 10^2, 10^3$ C and $q_D = -10^{-3}$ C. The *horizontal line* is the average. The initial discharge is the same for all of the scenarios

6 Model problem: discharge interaction with an external charged infinite sheet source

As a model problem, we employ a simple external electric field. Accordingly, consider an external electric field generated by *infinite flat sheet source*, governed by Gauss' law (Fig. 6):

$$\underbrace{\int_A \boldsymbol{D} \cdot \boldsymbol{n}\, dA}_{=\epsilon E 2A} = \int_V Q\, dV = \int_A Q_A\, dA = q_A A, \qquad (6.1)$$

where q_A is the charge per unit surface area, leading to

$$\boldsymbol{E} = \frac{q_A}{2\epsilon}\boldsymbol{n} = \boldsymbol{E}^{ext}, \qquad (6.2)$$

where $\boldsymbol{n}$ is the normal-outward unit vector from the flat plane.[3]

[3] All electric fields $\left(\left(\boldsymbol{E}^{ext}(t) + \sum_{j=1, j\neq i}^{N} \boldsymbol{E}_j(\boldsymbol{r}_i(t))\right)\right.$ are superposed to produce the righthand side "load" in Eq. 2.1.

6.1 Parameter selection

As an example, for a parameter set (below), 100 realizations were simulated, with the same starting conditions, but different feasible random pathways. *The system parameters were chosen for illustration purposes, and were not intended to simulate a specific natural or industrial scenario:*[4]

- The starting location of the discharge: $\boldsymbol{r}(t = 0) = (0, 0, 10^3)$ m,
- The external field location for a flat sheet: $\boldsymbol{r}_E = (0, 0, 0)$ m as in Fig. 7,
- Initial total system discharge: $q_D = -10^{-3}$ C.
- Sheet charge, varied: $q_A = 10^{-2}, 10^{-1}, 1, 10, 10^2, 10^3$ C or in nondimensional form $\frac{q_A}{|q_D|} = 10, 10^2, 10^3, 10^4, 10^5, 10^6$.
- The initial velocity of the discharge: $\boldsymbol{v}(t = 0) = (0, 0, -2 \times 10^5)$ m/s.
- The permittivity of the atmosphere: $\epsilon = 1.00059 \times \epsilon_o$, where $\epsilon_o = 8.8541878176 \times 10^{-12}$ F/m.
- The time-step size: $\Delta t = \frac{0.1}{||\boldsymbol{v}(t=0)||}$.
- The cone tolerance (for Eq. 4.1): $tol = 0.85$.

6.2 Discharge statistics

The frames in Fig. 7 illustrate the variation in branching for $N = 100$ random realizations, for each level of q_A. A relevant quantity is the radius of the circle ($\mathcal{R}$) that encompasses all of the branch strikes on the flat surface ($z = 0$). Specifically, we define the excursion ($\mathcal{R}$) away from the z-axis via

$$\mathcal{R} \stackrel{\text{def}}{=} max\sqrt{r_x^2 + r_y^2}, \tag{6.3}$$

where r_x and r_y are the maximum deviations in the x and y directions from the vertical (z axis). Statistically, the results in Fig. 8 can be described by computing the average ($\mathcal{A}$)

$$\mathcal{A} \stackrel{\text{def}}{=} \frac{1}{N}\sum_{i=1}^{N}\mathcal{R}_i \tag{6.4}$$

and standard deviation ($\mathcal{S}$)

$$\mathcal{S} \stackrel{\text{def}}{=} \sqrt{\frac{1}{N}\sum_{i=1}^{N}(\mathcal{R}_i - \mathcal{A})^2}. \tag{6.5}$$

Table 1 provides information on the excursion's dependence on the flat source charge magnitude. Clearly, the excursion decreases with the strength of the flat source electric field, which is dictated by q_A (see Figs. 7, 8). As the external (attractive) electric field increases, the magnitude of stochastic nature of the branching diminishes. For this model problem, this occurs for a ratio approximately $q_A/|q_D| \approx 10^3\,\text{m}^{-2}$. Of course, for other system settings, this threshold would be different. All simulations were run on a standard laptop with a code written by the author.

[4] We set the number of potential chances to branch along a pathway to 20. The total discharge mass was set to $m_D = 10^{-2}$ kg which represents all of the system mass (the charged electronic gas).

Table 1 The statistics as a function of q_A for $q_D = -10^{-3}$ C

Surface charge: q_A	Ratio: $\frac{q_A}{\vert q_D\vert}$	Mean: $\mathcal{A}$	SD: $\mathcal{S}$
10^{-2}	10	967.755	165.052
10^{-1}	10^2	658.985	111.670
1	10^3	136.393	21.226
10	10^4	17.394	2.352
10^2	10^5	5.406	0.891
10^3	10^6	1.719	0.326

7 Summary

In summary, a simple computational model and simulation framework was developed to describe the propagation and branching of electrical discharges in gaseous atmospheres. The framework allows analysts to rapidly simulate thousands of electrical discharge scenarios, in order to explore which parameters significantly affect the system behavior. The model is easy to encode and allows analysts to conduct numerous statistical sensitivity studies. As indicated, the algorithm is based physically on *dielectric breakdown*. Essentially, the charges at a branch tip build up and then plow through the atmosphere, resulting in multiple new pathways. In the case of natural atmospheric discharges (lightning), Earth-generated electrical field distributions can be found in Volland [67], Markson [68], MacGorman and Rust [69], Uman [70] and Rakov and Uman [1]. Measurements of local variations in relevant atmospheric property data can be found in, for example, Bering et al. [71], Holzworth et al. [72], Pinto et al. [73], Hu et al. [74]. Also, of course, there are many industrially relevant machinery-generated external electric fields possible, such as:

- **An electric field due to charged external point source** (Fig. 9), which is governed by Gauss' law:

$$\underbrace{\int_A \boldsymbol{D}\cdot\boldsymbol{n}\,dA}_{=\epsilon E 4\pi||\boldsymbol{r}-\boldsymbol{r}_o||^2} = \int_V Q\,dV = q_p \Rightarrow \boldsymbol{E} = \frac{q_p}{4\pi\epsilon||\boldsymbol{r}-\boldsymbol{r}_o||^2}\boldsymbol{n}, \tag{7.1}$$

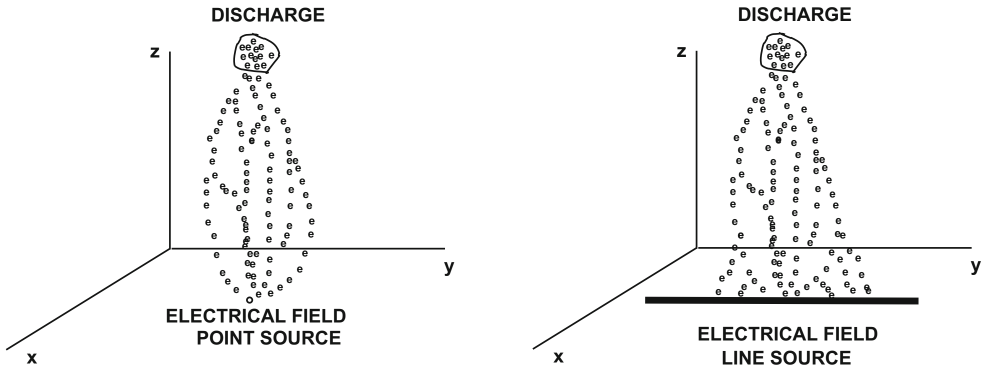

Fig. 9 *Left* Example of a point-source term. *Right* Example of a line-source term

where q_p is the charge at a point, $\boldsymbol{n}$ is the normal-outward unit vector and $||\boldsymbol{r} - \boldsymbol{r}_o||$ is the distance from the point source.

- **An electric field due to a charged external conducting wire source** (Fig. 9), idealized by an (extremely thin cylinder) source, governed by Gauss' law:

$$\underbrace{\int_A \boldsymbol{D} \cdot \boldsymbol{n}\, dA}_{=\epsilon E 2\pi ||\boldsymbol{r}-\boldsymbol{r}_o|| L} = \int_V Q\, dV = \int_L Q_L\, dL = q_L L$$
$$\Rightarrow \boldsymbol{E} = \frac{q_L}{2\pi\epsilon ||\boldsymbol{r} - \boldsymbol{r}_o||}\boldsymbol{n}, \quad (7.2)$$

where q_L is the charge per unit length, $\boldsymbol{n}$ is the radially-outward (to the cylinder) unit vector and $||\boldsymbol{r} - \boldsymbol{r}_o||$ the radial distance from the line source.

Of course one can generate more complex fields for other structures numerically, for example using Finite Difference Time Domain Methods or Finite Element Methods. Generally speaking, the specific directions subbranches of the local branching pathways are somewhat random, due to the interaction with the surrounding gaseous atmosphere, with influence coming from the ambient electrical field of the environment. More detailed simulation of ion and electron flows, taking into account all of the charged species which comprise a branch, would require billions or trillions of interacting degrees of freedom, which is computationally intractable for practical use. Thus, so-called multiscale approaches, which utilize simplified models, such as the model presented in this paper, for the bulk of the calculations, but detailed models for ion and electron interaction and dielectric breakdown models at the branch front tip are a viable way forward. Large-scale particle interaction models have been extensively studied, other types of particulate systems, in Onate et al. [75–77], Rojek et al. [78], Carbonell et al. [79], Labra and Onate [80], Leonardi et al. [81], Cante et al. [82], Rojek [83], Bolintineanu et al. [84], Avci and Wriggers [85] and Zohdi [29–33,86–93] and is a topic of current investigation by the author.

Acknowledgements The author gratefully acknowledges the generous support of the Siemens corporation during the course of this research.

References

1. Rakov V, Uman M (2003) Lightning: physics and effects. Cambridge University Press, Cambridge
2. Demirkol MK, Inan US, Bell TF, Kanekal SG, Wilkinson DC (1999) Ionospheric effects of relativistic electron enhancement events. Geophys Res Lett 26(23):3557–3560
3. Uman MA (1986) All about lightning. Dover Publications, Inc., Mineola
4. Fishman GJ, Bhat PN, Malozzi R, Horack JM, Koshut T, Kouveliotou C, Pendleton GN, Meegan CA, Wilson RB, Paciesas WS, Goodman SJ, Christian HJ (1994) Discovery of intense gamma-ray flashes of atmospheric origin. Science 264:1313–1316
5. Inan US, Reising SC, Fishman GJ, Horack JM (1996) On the association of terrestrial gamma-ray bursts with lightning and implications for sprites. Geophys Res Lett 23(9):1017–1020
6. Inan US, Inan A (1999) Engineering electromagnetics. Addison Wesley, Boston
7. Staubach C, Wulff J, Jenau F (2012) Particle swarm based simplex optimization implemented in a nonlinear multiple-coupled finite-element-model for stress grading in generator end windings. In: Proceedings of the 2012 13th international conference on optimization of electrical and electronic equipment (OPTIM), pp 482–488, ISSN 1842-0133
8. Staubach C, Pohlmann F, Jenau F (2012) Comparison of transient time-domain and harmonic quasi-static solution of electrical and thermal coupled numerical stress grading calculations for large rotating machines. In: IEEE international symposium on electrical insulation (ISEI) conference record of the 2012, pp 209–213, ISSN 1089-084X
9. Staubach C, Kempen S, Pohlmann F, Jenau F (2011) Computer aided design of an end corona protection system for accelerated voltage endurance testing at increased line frequency. In: Proceedings of the 2011 electrical insulation conference (EIC), pp 170–174. doi:10.1109/EIC.2011.5996140
10. Staubach C, Kempen S, Pohlmann F (2010) Calculation of electric field distribution and temperature profile of end corona protection systems on large rotating machines by use of finite element model. In: Proceedings of the 2010 IEEE international symposium on electrical insulation, pp 1–6. doi:10.1109/ELINSL.2010.5549543

11. Mcdermid W (2015) Insulation-system diagnostics for rotating machines. IEEE Electr Insul Mag 29:24–33, 2013, ISSN 0883-7554
12. Merouchi A, David E, Baudoin F, Mary D, Fofana I (2015) Optimization of the electrical properties of epoxy-SiC composites for stress-grading application. In: Proceedings of the 2015 IEEE conference on electrical insulation and dielectric phenomena (CEIDP), pp 713–716
13. Merouchi A, David E, Baudoin F, Mary D, Fofana I (2015) Optimization of the electrical properties of epoxy-SiC composites for stress-grading application. In: Proceedings of the 2015 IEEE conference on electrical insulation and dielectric phenomena (CEIDP), pp 713–716. doi:10.1109/CEIDP.2015.7352140
14. Schmerling R, Jenau F, Staubach C, Pohlmann F (2012) Investigations of modified nonlinear electrical materials for end corona protection in large rotating machines. In: Proceedings of the 47th international universities power engineering conference (UPEC), pp 1–5. doi:10.1109/UPEC.2012.6398563
15. Weida D, Bhmelt S, Clemens M (2010) Design of ZnO microvaristor end corona protection for electrical machines. In: Proceedings of the 2010 IEEE international symposium on electrical insulation, pp 1–4. doi:10.1109/ELINSL.2010.5549550
16. Day WJ, Wroblewski HA, Weddleton RA (1976) End turn corona suppressing coatings their composition and effect. In: Proceedings of the 1976 IEEE international conference on electrical insulation, pp 103–105. doi:10.1109/EIC.1976.7464178
17. Kogan V, Dawson F, Gao G, Nindra B (1995) Surface corona suppression in high voltage stator winding end turns. In: Proceedingsof the electrical electronics insulation conference and electrical manufacturing and coil winding conference, pp 411–415. doi:10.1109/EEIC.1995.482397
18. Liu Y, Xu C (2000) Optimum design on anti-corona coating of high voltage generator coil ends. In: Proceedings of the 6th international conference on properties and applications of dielectric materials (Cat. No.00CH36347). IEEE conference publications, vol 2, pp 967–969. doi:10.1109/ICPADM.2000.876391
19. Taylor N (2015) Measured and modeled capacitance, loss and harmonics in stator insulation with nonlinear stress control. IEEE Trans Dielectr Electr Insul 22(6):3133–3145. doi:10.1109/TDEI.2015.005260
20. Krpal O, Kuerov E (2014) Comparison of voltage distribution in end-winding of synchronous generator. In: Proceedings of the 2014 15th international scientific conference on electric power engineering (EPE), pp 575–578. doi:10.1109/EPE.2014.6839410
21. Sumereder C, Muhr M, Senn F, Grubelink W, Marek P (2008) Thermal and lifetime behavior of innovative insulation systems for rotating machines. In: Proceedings of the 2008 18th international conference on electrical machines, pp 1–4. doi:10.1109/ICELMACH.2008.4799975
22. Hudon C, Rehder RH (1995) Recognition of phase resolved partial discharge patterns for internal discharges and external corona activity. In: Proceedings of 1995 IEEE 5th international conference on conduction and breakdown in solid dielectrics, pp 386–392. doi:10.1109/ICSD.1995.523014
23. Abdel-Salam M, Shamloul D (1992) Computation of ion-flow fields of AC coronating wires by charge simulation techniques. IEEE Trans Electr Insul 27(2):352–361. doi:10.1109/14.135606
24. Litinsky A, Schmidt G, Pohlmann F, Hirsch H (2016) Analysis of resistance characteristics of multilayered field grading material structures on rotating machines. In: Proceedings of the 2016 IEEE international conference on dielectrics (ICD), vol 1, pp 426–430, doi:10.1109/ICD.2016.7547634
25. Guastavino F, Cordano D, Torello E, Della Giovanna L (2016) PD evolution of conventional and corona resistant enamels. In: Proceedings of the 2016 IEEE conference on electrical insulation and dielectric phenomena (CEIDP), pp 259–262. doi:10.1109/CEIDP.2016.7785686
26. Ou C, Techaumnat B (2016) Study on particle-induced corona discharge in insulation systems. In: Proceedings of the 2016 13th international conference on electrical engineering/electronics, computer, telecommunications and information technology (ECTI-CON), pp 1–6. doi:10.1109/ECTICon.2016.7561319
27. Bouhaouche M, Mekhaldi A, Teguar M (2016) Evaluation of electric field distribution on a 400 kV composite insulator under various service conditions. In: Proceedings of the 2016 IEEE international conference on dielectrics (ICD), pp 1003–1006. doi:10.1109/ICD.2016.7547787
28. Nazir MT, Phung BT (2016) AC corona resistance performance of silicone rubber composites with micro/nano silica fillers. In: Proceedings of the 2016 IEEE international conference on dielectrics (ICD), vol 2, pp 681–684. doi:10.1109/ICD.2016.7547707
29. Zohdi TI (2009) Dielectric breakdown elimination via particulate additives. Int J Fract Lett Micromech 159:L247–L253
30. Zohdi TI (2010a) Localized electrical current propagation in stochastically perturbed atmospheres. Int J Numer Methods Eng 84:27–46
31. Zohdi TI (2010b) Simulation of coupled microscale multiphysical-fields in particulate-doped dielectrics with staggered adaptive FDTD. Comput Methods Appl Mech Eng 199:79–101
32. Zohdi TI (2011) Joule-heating field phase-amplification in particulate-doped dielectrics. Int J Eng Sci 49:30–40
33. Zohdi TI (2012) Estimation of electrical-heating load-shares for sintering of powder mixtures. Proc R Soc 468:2174–2190
34. Azevedo RG, Jones DG, Jog AV, Jamshidi B, Myers DR, Chen L, Fu X-A, Mehregany M, Wijesundara MBJ, Pisano AP (2007) A SiC MEMS resonant strain sensor for harsh environment applications. IEEE Sens J 7(4):568–576
35. Schwartz SW, Myers DR, Kramer RK, Choi S, Jordan A, Wijesundara MBJ, Hopcroft MA, Pisano AP (2008) Silicon and silicon carbide survivability in an in-cylinder combustion environment. PowerMEMS 2008, Sendai, Japan, Nov 9–12
36. Ikeda Y, Nishiyama A, Kaneko M (2009) Microwave enhanced ignition process for fuel mixture at elevated pressure of 1 MPa. In: Proceedings of the 47th AIAA aerospace sciences meeting including the new horizons forum and aerospace exposition 5–8 Jan 2009, Orlando
37. Ikeda Y, Nishiyama A, Kawahara N, Tomita E, Nakayama T (2006) Local equivalence ratio measurement of CH4/air and C3H8/air laminar flames by laser-induced breakdown spectroscopy. In: Proceedings of the 44th AIAA aerospace sciences meeting and exhibit, 9–12 Jan 2006, Reno, Nevada, AIAA Paper No. 2006-965
38. Leipold F, Stark RH, El-Habachi A, Schoenbach KH (2000) Electron density measurements in an atmospheric pressure air plasma by means of IR heterodyne interferometry. J Phys D Appl Phys 33:2268–2273
39. Phelps AV (1987) Excitation and ionization coefficients. In: Christophourou LG, Bouldin DW (eds) Gaseous di-electrics V. Pergamon, New York
40. Aleiferis PG, Taylor AMKP, Whitelaw JH, Ishii K, Urata Y (2000) Cyclic variations of initial flame kernel growth in a Honda VTEC-E lean-burn spark-ignition engine. SAE Paper No. 2000-01-1207
41. Johansson B (1996) Cycle to cycle variations in SI engines: the effects of fluid flow and gas composition in the vicinity of the spark plug on early combustion. SAE Paper 962084
42. Kogoma M (2003) Generation of atmospheric-pressure glow and its applications. J Plasma Fusion Res 79(10):1000
43. Phuoc T (2000) Single-point versus multi-point laser ignition: experimental measurements of combustion times and pressures. Combust Flame 122:508–510

44. Phuoc T (2000) Laser spark ignition: experimental determination of laser-induced breakdown thresholds of combustion gases. Opt Commun 175:419–423
45. Morsy MH, Ko YS, Chung SH, Cho P (2001) Laser-induced two point ignition of premixture with a single-shot laser. Combust Flame 125:724–727
46. Morsy MH, Chung SH (2003) Laser induced multi-point ignition with a single-shot laser using two conical cavities for hydrogen/air mixtures. Exp Therm Fluid Sci 27:491–497
47. Ma JX, Alexander DR, Poulain DE (1998) Laser spark ignition and combustion characteristics of methane-air mixtures. Combust Flame 112:492–506
48. Ma JX, Ryan TW, Buckingham JP (1998) Nd:YAG laser ignition of natural gas. ASME, 98-ICE-114
49. Mohamed AH, Block R, Schoenbach KH (2002) Direct current discharges in atmospheric air. IEEE Trans Plasma Sci 30(1):182–183
50. Weinberg FJ, Wilson JR (1971) A preliminary investigation of the use of focused laser beams for minimum ignition energy studies. Proc R Soc Lond A321:41–52
51. Dale JD, Smy PR, Clements RM (1978) Laser ignited internal combustion engine: an experimental study. SAE-780329, Detroit
52. Ronney PD (1994) Laser versus conventional ignition of flames. Opt Eng 33(2):510
53. Beduneau JL, Kim B, Zimmer L, Ikeda Y (2003) Measurements of minimum ignition energy in premixed laminar methane/air flow by using laser induced spark. Combust Flame 132:653–665
54. Chen YL, Lewis JWL (2001) Visualisation of laser-induced breakdown and ignition. Opt Express 9(7):360–372
55. Kim Y, Ferreri VW, Rosocha LA, Anderson GK, Abbate S, Kim K-T (2006) Effect of plasma chemistry on activated propane/air flames. IEEE Trans Plasma Sci 34(6):2532–2536
56. Ombrello T, Ju Y (2007) Ignition enhancement using magnetic gliding arc. In: Proceedings of the 45th AIAA aerospace sciences meeting and exhibit, 8–11 Jan, Reno, Nevada, AIAA Paper No. 2007-1025
57. Mintoussov E, Anokhin E, Starikovskii AY (2007) Plasma-assisted combustion and fuel reforming. In: Proceedings of the 45th AIAA aerospace sciences meeting and exhibit, 8–11 Jan 2007, Reno, Nevada, AIAA Paper No. 2007-1382
58. Korolev YD, Matveev IB (2006) Nonsteady-state processes in a plasma pilot for ignition and flame control. IEEE Trans Plasma Sci 34(6):2507
59. Esakov II, Grachev LP, Khodataev KV, Vinogradov VV, Van Wie DM (2006) Propane-air mixture combustion assisted by MW discharge in a speedy airflow. IEEE Trans Plasma Sci 34(6):2497
60. Linkenheil K, Ruoss RO, Heinrich W (2004) Design and evaluation of a novel spark-plug based on a microwave coaxial resonator. Microwave conference. 34th European, vol 3, pp 1561–1564
61. Linkenheil K, Ruoss HO, Grau T, Seidel J, Heinrich W (2005) A novel spark-plug for improved ignition in engines with gasoline direct injection (GDI). IEEE Trans Plasma Sci 33(5):1696
62. Kawahara K, Ueda K, Ando H (1998) Mixing control strategy for engine performance improvement in a gasoline direct-injection engine. SAE Paper, No. 980158
63. Mehresh P, Souder J, Flowers D, Riedel U, Dibble RW (2005) Combustion timing in HCCI engines determined by ion-sensor: experimental and kinetic modeling. Proc Combust Inst 30:2701–2709
64. Bogin G, Chen JY, Dibble RW (2008) The effects of intake pressure, fuel concentration, and bias voltage on the detection of ions in a Homogeneous Charge Compression Ignition (HCCI) engine. Proc Combust Inst 32(2):2877–2884
65. Prager J, Riedel U, Warnatz J (2007) Modeling ion chemsitry and charged species diffusion in lean methane-oxygen flames. Proc Combust Inst 31(1):1129–1137
66. Townsend JS (1914) Electricity in gases. Oxford University Press, Oxford
67. Volland H (1984) Atmospheric electrodynamics. In: Lanzerotti LJ, Wasson JT (eds) Physics in chemistry and space, vol II, 205th edn. Springer, New York
68. Markson R (1976) Ionospheric potential variations obtained from aircraft measurements of potential gradient. J Geophys Res 84:161–200
69. MacGorman DR, Rust WD (1998) The electrical nature of thunderstorms. Dover, New York
70. Uman MA (1974) The earth as a leakey spherical capacitor. Am J Phys 42:1033–1035
71. Bering EA, Rosenberg TJ, Benbrook JR, Detrick D, Matthews DL, Rycroft MJ, Saunders MA, Sheldon WR (1980b) Electrical fields, electron precipitation, and VLF radiation during a simultaneous magnetospheric substorm and atomospheric thunderstorm. J Geophys Res 85:55–72
72. Holzworth RH, Norville KW, Kintner PM, Power SP (1986) Stratospheric conductivity variations over thunderstorms. J Geophys Res 93:13257–13263
73. Pinto IRCA, Pinto O, Gonzalez WD, Dutra LG, Wygant J, Mozer FS (1988) Stratospheric electric field and conductivity measurements over electrified convective clouds in the South American region. Geophys Res 93:709–715
74. Hu H, Holzworth RH, Li YQ (1989) Thunderstorm related variations in stratospheric conductivity measurements. J Geophys Res 94(16):429–435
75. Onate E, Idelsohn SR, Celigueta MA, Rossi R (2008) Advances in the particle finite element method for the analysis of fluid-multibody interaction and bed erosion in free surface flows. Comput Methods Appl Mech Eng 197(19–20):1777–1800
76. Onate E, Celigueta MA, Idelsohn SR, Salazar F, Surez B (2011) Possibilities of the particle finite element method for fluid-soil-structure interaction problems. Comput Mech 48:307–318
77. Onate E, Celigueta MA, Latorre S, Casas G, Rossi R, Rojek J (2014) Lagrangian analysis of multiscale particulate flows with the particle finite element method. Comput Part Mech 1(1):85–102
78. Rojek J, Labra C, Su O, Onate E (2012) Comparative study of different discrete element models and evaluation of equivalent micromechanical parameters. Int J Solids Struct 49:1497–1517. doi:10.1016/j.ijsolstr.2012.02.032
79. Carbonell JM, Onate E, Suarez B (2010) Modeling of ground excavation with the particle finite element method. J Eng Mech ASCE 136:455–463
80. Labra C, Onate E (2009) High-density sphere packing for discrete element method simulations. Commun Numer Methods Eng 25(7):837–849
81. Leonardi A, Wittel FK, Mendoza M, Herrmann HJ (2014) Coupled DEM-LBM method for the free-surface simulation of heterogeneous suspensions. Comput Part Mech 1(1):3–13
82. Cante J, Davalos C, Hernandez JA, Oliver J, Jonsen P, Gustafsson G, Haggblad HA (2014) PFEM-based modeling of industrial granular flows. Comput Part Mech 1(1):47–70
83. Rojek J (2014) Discrete element thermomechanical modelling of rock cutting with valuation of tool wear. Comput Part Mech 1(1):71–84
84. Bolintineanu DS, Grest GS, Lechman JB, Pierce F, Plimpton S, Schunk PR (2014) Particle dynamics modeling methods for colloid suspensions. Comput Part Mech 1(3):321–356
85. Avci B, Wriggers P (2012) A DEM-FEM coupling approach for the direct numerical simulation of 3D particulate flows. J Appl Mech 79:010901-1
86. Zohdi TI (2004a) A computational framework for agglomeration in thermo-chemically reacting granular flows. Proc R Soc 460:3421–3445

87. Zohdi TI (2004b) Modeling and direct simulation of near-field granular flows. Int J Solids Struct 42(2):539–564
88. Zohdi TI (2005) Charge-induced clustering in multifield particulate flow. Int J Numer Methods Eng 62(7):870–898
89. Zohdi TI (2007) Computation of strongly coupled multifield interaction in particle-fluid systems. Comput Methods Appl Mech Eng 196:3927–3950
90. Zohdi TI (2008) On the computation of the coupled thermo-electromagnetic response of continua with particulate microstructure. Int J Numer Methods Eng 76:1250–1279
91. Zohdi TI (2010c) On the dynamics of charged electromagnetic particulate jets. Arch Comput Methods Eng 17(2):109–135
92. Zohdi TI (2014) Embedded electromagnetically sensitive particle motion in functionalized fluids. Comput Part Mech 1:27–45
93. Zohdi TI (2016) On progressive blast envelope evolution of charged particles in electromagnetic fields. Comput Methods Appl Mech Eng. doi:10.1016/j.cma.2016.05.003